CIMAC CONGRESS 25
ZURICH, MAY 19 – 23, 2025

2025 | 443

Life and Reliability Analysis of Marine Engine Piston Ring Based on Tribo-dynamic Model

Tribology

Lining Gao, Shanghai Jiao Tong University

Zhaohui Xu, Shanghai Jiao Tong University
Shuo Liu, Shanghai Jiao Tong University
Bohong Zhang, Shanghai Jiao Tong University
YI CUI, Shanghai Jiaotong University

DOI: https://doi.org/10.5281/zenodo.15230981

ABSTRACT

Piston rings play a crucial role in sealing, heat conduction, lubrication, and other essential functions, significantly impacting the overall reliability of the engine. Wear is the primary failure mode of piston rings, influenced by multiple sources of uncertainty such as material properties and operating conditions, posing challenges to life prediction and reliability analysis. In this study, focusing on piston rings of a medium speed marine engine, the average Reynolds equation is used to describe lubrication behavior. A three-dimensional ring tribo-dynamic model is established, solved using the finite element method in space and the backward Euler method in time. Wear under mixed lubrication is calculated based on the Greenwood-Tripp contact theory and Archard equation. Furthermore, Latin hypercube sampling is used to obtain tribo-dynamics calculation input that takes into account multi-source uncertainty factors such as materials and working condition parameters, and piston ring wear sample data can be obtained through model calculations. Finally, a surrogate model is developed to relate multiple sources of uncertainty to wear data, conducting a reliability analysis to determine wear life at different reliability levels, thereby providing support for high-reliability design of piston rings.

1 INTRODUCTION

With increasingly stringent emission regulations, the power density and thermal efficiency of internal combustion engines (ICEs) have been steadily improving. The piston ring-cylinder liner system (PRCL), as a critical reciprocating friction pair in ICEs, is facing increasingly severe mechanical and thermal loads. Operating under harsh conditions over extended periods, piston rings perform essential functions such as sealing, lubrication, and heat conduction, with their performance directly influencing the reliability and durability of the entire engine. However, wear, as the primary failure mode of piston rings, is often influenced by multiple uncertain factors, such as material properties and operating conditions. This makes failure prediction and reliability analysis particularly challenging.

To perform reliability calculations and lifetime predictions for piston rings, it is essential to first obtain accurate wear depth, which relies on refined tribological simulation models. Early studies on the piston ring-cylinder liner system (PRCL) primarily focused on developing one-dimensional line-contact lubrication models, often neglecting surface roughness and deformation effects caused by oil film pressure. For instance, Dowson et al. [1] proposed a one-dimensional elastohydrodynamic (EHD) model that considered deformations of the cylinder liner and piston ring surfaces caused by high-pressure fluid. Their calculations indicated that elastic deformation could increase the minimum oil film thickness.

To date, the working characteristics of the PRCL friction pair have been extensively studied. Various factors, such as elastic deformation [4–8], lubricant rheology [9–13], surface texturing [14–19], surface roughness [20–22], and cavitation effects [23–27], have been adequately incorporated into existing computational models based on the average Reynolds equation proposed by Patir and Cheng [2,3]. These models have played a significant role in evaluating the tribological properties of the PRCL system. Additionally, since the piston ring directly withstands the combustion gas load during engine operation, the temperature field significantly affects the tribological characteristics of the PRCL system, as noted in many studies [28–30]. However, the aforementioned models are often developed for two-dimensional piston ring cross-sections, and studies on three-dimensional tribo-dynamic coupling models for piston rings are scarce. As a three-dimensional flexible body, the tribological characteristics of the piston ring vary significantly at different circumferential positions. Consequently, the wear depth also differs across positions, which has a substantial impact on reliability calculations and lifetime predictions.

To address the aforementioned issues, this study develops a three-dimensional tribo-dynamic coupling model for piston rings based on the finite element method. The average Reynolds equation is employed to describe the lubrication characteristics of the thin oil film, and it is coupled with the dynamic equations of the three-dimensional flexible piston ring for solving. This approach enables the determination of the wear distribution across the three-dimensional piston ring. Furthermore, by incorporating multi-source uncertainties such as material properties, elastic forces, and operating conditions into the failure mechanism model, the cyclic wear volume of the piston ring and its statistical distribution patterns are analyzed. Reliability analysis is then conducted to derive the wear life under different reliability levels. This research provides theoretical support for the design of high-reliability piston rings.

2 TRIBO-DYNAMIC MODEL

This section provides a detailed introduction to the construction methods of lubrication and dynamic models, as well as the calculation method for wear depth under mixed lubrication conditions.

2.1 Lubrication

The Reynolds equation describes the lubrication characteristics of thin oil film and has been widely applied in tribology studies of PRCL conjunctions. To further account for the effect of surface roughness on lubrication flow, this study adopts the averaged Reynolds equation proposed by Patir and Cheng [27] as the governing equation:

$$\frac{\partial}{\partial x}\left(\phi_x \frac{h^3}{12\mu}\frac{\partial p}{\partial x}\right)+\frac{\partial}{\partial y}\left(\phi_y \frac{h^3}{12\mu}\frac{\partial p}{\partial y}\right)= -\frac{u}{2}\left[\phi_c \frac{\partial h}{\partial y}+\sigma\frac{\partial \phi_s}{\partial y}\right]+\phi_c \frac{\partial h}{\partial t} \tag{1}$$

where μ represents the dynamic viscosity of the lubricant. x and y are the local circumferential and axial coordinate axes, respectively, as shown in Figure 1. ϕ_x and ϕ_y are the pressure flow factors, ϕ_s is the shear flow factor, and ϕ_c is the contact factor [9]. h and p denote the oil film thickness and pressure, respectively, u is the piston ring velocity, σ is the composite surface roughness, and t represents time.

In addition to the normal pressure p described above, the friction force generated by fluid shear also acts on the piston ring surface. Its

calculation formula is as follows:

$$\tau = -\frac{\mu u}{h}\left(\phi_f + \phi_{fs}\right) - \phi_{fp}\frac{h}{2}\frac{\partial p}{\partial y} \quad (2)$$

where ϕ_f , ϕ_{fs} and ϕ_{fp} are the shear stress factors.

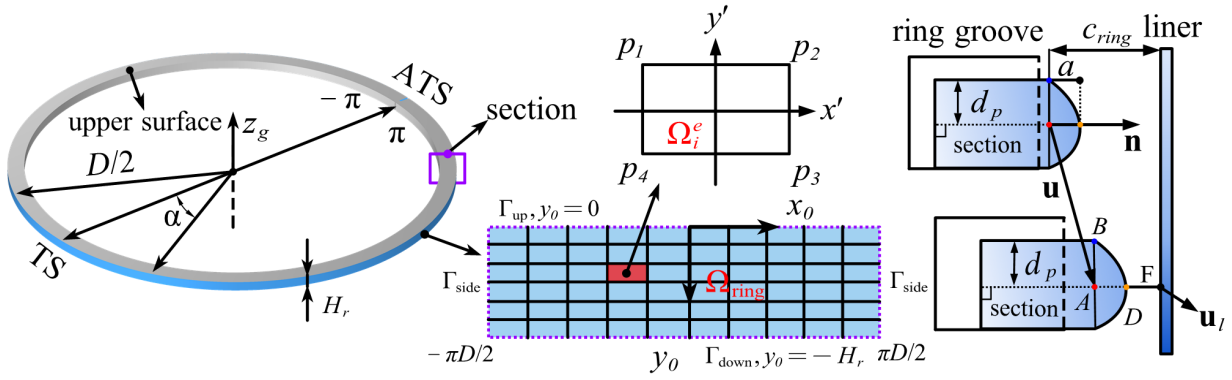

Figure 1. Piston ring lubrication domain diagram

Establishing the film thickness expression is a necessary condition for solving the averaged Reynolds equation. Figure 1 illustrates the lubrication domain of the piston ring. Point A is a point on the ring surface, with coordinates (x,y,z), and $\mathbf{n}(x,y,z)$ represents its normal direction. $\mathbf{u}(x,y,z,t)$ denotes its global displacement vector. $\mathbf{u}(x,y,z,t)$ includes the piston ring's displacement and deformation, whose normal component to the surface in the lubrication domain alters the oil film thickness. F is the corresponding point of A on the straight line, with coordinates (x_l,y_l,z_l,t), and $\mathbf{u}_l$ represents its displacement vector.

In this study, the profile is described by a quadratic polynomial, and the expression for the oil film thickness on the piston ring surface can be written as:

$$h_{ring} = c_{ring} - \frac{a}{d_{pm}^2}(z_B - z)(z_B - z - 2d_{pm}) - \mathbf{u}(x,y,z,t)\cdot\mathbf{n}(x,y,z) + \mathbf{u}_l(x_l,y_l,z_l,t)\cdot\mathbf{n}(x,y,z) \quad (3)$$

where a represents the maximum profile height, and d_p denotes the distance from point A to the upper surface of the ring. When point D coincides with the highest point of the profile, d_p becomes d_{pm}. Unfolding the piston ring surface results in a two-dimensional lubrication domain with a length of πD and a height of H_r. A solution coordinate system (x_0,y_0) is established on the piston ring surface, and the cylinder liner surface coordinates are represented as (x_2,y_2). The mapping between the global coordinate system and the local lubrication coordinate system can be achieved through the mesh node indices. Thus, the oil film thickness can also be expressed in the following form:

$$h_{ring} = c_{ring} + h_{p\text{-}ring}(x_0,y_0) + d_1^{ring}(x_0,y_0,t) + d_2^{ring}(x_2,y_2,t) \quad (4)$$

where c_{ring} represents the initial clearance when the ring profile is absent, which is used to improve the convergence of the calculation. $h_{p\text{-}ring}(x_0,y_0)$ denotes the profile height of the ring, $d_1^{ring}(x_0,y_0,t)$ represents the influence of the flexible piston ring's dynamic behavior on the film thickness, and $d_2^{ring}(x_2,y_2,t)$ accounts for the deformation of the cylinder liner. Since high-pressure gases exist on both the top and bottom sides of the piston ring, the boundary conditions for solving Equation (1) are as follows:

$$\begin{cases} p(x,y) = P_1, (x,y) \in \Gamma_{up} \\ p(x,y) = P_2, (x,y) \in \Gamma_{down} \\ \partial p / \partial n = 0, (x,y) \in \Gamma_{side} \end{cases} \quad (5)$$

2.2 Wear calculation

In addition to the fluid load, when the oil film is insufficient to support the load on the piston ring, direct asperity contact occurs between the ring and cylinder liner surfaces. According to the Greenwood-Tripp [31] contact theory, the asperity contact pressure can be calculated using the following equation:

$$p_{asp} = (16\sqrt{2}/15)\pi(\eta\beta\sigma)^2 E\sqrt{\frac{\sigma}{\beta}}F_{5/2}\left(\frac{h}{\sigma}\right) \quad (6)$$

where $E' = \left((1-v_{ring}^2)/E_{ring} + (1-v_{liner}^2)/E_{liner}\right)^{-1}$ is the composite Young's modulus. E_{ring} and E_{liner} are the Young's moduli of the ring and cylinder liner, respectively, and v_{ring} and v_{liner} are their Poisson's ratios. $F_n(H)$ represents the asperity height distribution function of the contact surfaces. In addition to the normal contact force described above, asperities generate additional frictional

forces during tangential relative motion [32,33].

$$f = \tau_0 a_c + m p_{asp} \tag{7}$$

In this study, the Archard model is used to calculate the wear of the three-dimensional piston ring under mixed lubrication. According to this law, the wear volume depends on the normal load, sliding distance, and material hardness. The calculation expression can be written as:

$$V = K_w \frac{W}{H} S \tag{8}$$

where V represents the wear volume, K_w is the material wear coefficient, W denotes the normal load, and S is the sliding distance. When calculating wear under mixed lubrication conditions, wear occurs only in the asperity contact regions, while other areas of the piston ring and cylinder liner surfaces are completely separated by the lubricant film. By transforming the above equation, the formula for the incremental wear depth can be expressed as:

$$\Delta h = K_w \frac{p_{asp}}{H} s \tag{9}$$

in the above equation, Δh represents the wear increment during a specific time step, p_{asp} denotes the asperity contact pressure, and s is the sliding distance within the time step. In this study, the above equation is integrated over a single engine cycle to calculate the cycle wear depth:

$$h_{cw} = \int_{t=0}^{T_{cycle}} K_w \frac{p_{asp}}{H} s \; dt \tag{10}$$

where h_{cw} represents the cycle wear depth, and T_{cycle} denotes the duration of one engine cycle. When calculating wear, the actual measured surface hardness and wear coefficient of the ring should be used, with particular attention given to the coating of the piston ring.

2.3 Dynamics

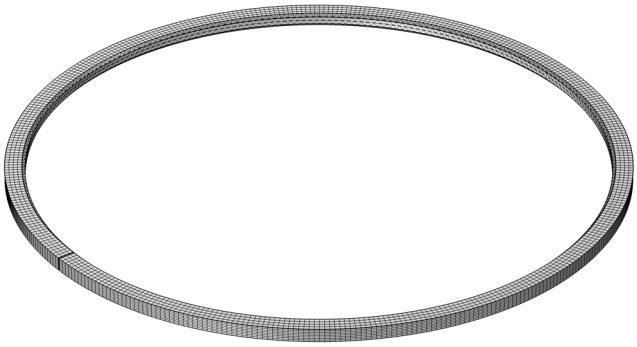

Figure 2. Three-Dimensional Piston Ring Mesh

To establish the dynamics model of a three-dimensional flexible body, as shown in Figure 2, the finite element method is employed in this study to discretize the piston ring. Within each discretized element, the displacement field can be interpolated using the basis functions $\mathbf{N}^e$ and the nodal displacement vector $\mathbf{u}^e$.

$$\mathbf{u} = \mathbf{N}^e \mathbf{u}^e \tag{11}$$

Substituting it into the equilibrium differential equation of the flexible body and rearranging yields:

$$\mathbf{M}^e \ddot{\mathbf{u}}^e + \mathbf{K}^e \mathbf{u}^e = \mathbf{Q}^e \tag{12}$$

where $\mathbf{M}^e = \int_{V_e} \rho \mathbf{N}^{e\mathrm{T}} \mathbf{N}^e \mathrm{d}V$ is the element mass matrix, $\mathbf{K}^e = \int_{V_e} \mathbf{B}^{\mathrm{T}} \mathbf{D} \mathbf{B} \mathrm{d}V$ is the element stiffness matrix, and $\mathbf{Q}^e$ is the element load vector. By assembling all the elements of the piston ring, the structural dynamic equation of the piston ring can be obtained as:

$$\mathbf{M}\ddot{\mathbf{q}} + \mathbf{K}\mathbf{q} = \mathbf{Q} \tag{13}$$

where $\mathbf{M}$, $\mathbf{K}$, and $\mathbf{Q}$ represent the system's mass matrix, stiffness matrix, and load vector, respectively. Furthermore, by introducing Rayleigh damping $\mathbf{D} = \alpha \mathbf{M} + \beta \mathbf{K}$ to simplify the actual structural damping, the Equation (13) can be rewritten as:

$$\mathbf{M}\ddot{\mathbf{q}} + \mathbf{D}\dot{\mathbf{q}} + \mathbf{K}\mathbf{q} = \mathbf{Q} \tag{14}$$

The equation (14) can be solved using the backward Euler method. The specific time-stepping scheme can be referred to in previous studies [34].

2.4 Coupled solving method

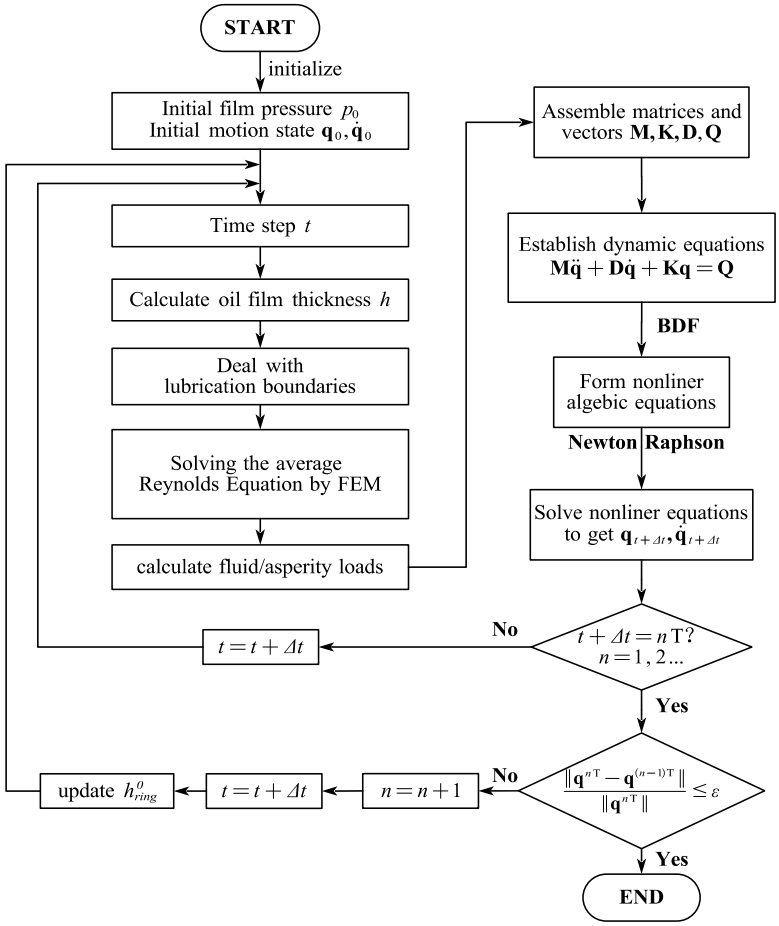

Figure 3. Coupling solution algorithm

The construction methods of the lubrication model and dynamic model for the PRCL system have been presented above. Due to the strong coupling relationship between the models, the governing equations must be solved iteratively in a coupled manner. The coupling solution algorithm proposed in this study is shown in Figure 3 and can be divided into the following main steps:

Step 1. Initialize Model Parameters. At the initial moment, the oil film pressure p in the lubrication model is set to zero. The velocity $\dot{\mathbf{q}}$ and acceleration $\ddot{\mathbf{q}}$ of the multibody system are also set to zero. The piston ring is assumed to be in an ideal assembly state.

Step 2. Solve the Lubrication Model. At any given time t, the oil film thickness is calculated based on the displacement and deformation information output from the dynamic model. The averaged Reynolds equation is then solved using the finite element method (refer to previous studies). Subsequently, the fluid load and asperity load acting on the dynamic model can be calculated based on the relevant equations.

Step 3. Solve the Dynamic Model. The fluid load and asperity load calculated in Step 2 are incorporated into the generalized load vector $\mathbf{Q}$. A time-stepping scheme is established using the backward differentiation formula (BDF), and the Newton-Raphson method is employed to iteratively calculate the velocity $\mathbf{q}^{t+\Delta t}$ and acceleration $\dot{\mathbf{q}}^{t+\Delta t}$ at the next moment.

Step 4. Time-Stepping. The $\mathbf{q}^{t+\Delta t}$ and $\dot{\mathbf{q}}^{t+\Delta t}$ values obtained from the previous step are input into the lubrication model for iterative calculations at the next time step (repeating Steps 2 and 3).

Step 5. Convergence Judgment. When the simulation time reaches an integer multiple of a single cycle, the results at the beginning and end of the cycle are compared to check if they meet the tolerance requirements. If convergence is achieved, the computation ends. Otherwise, the initial oil film thickness of the ring set is updated, and the iterative computation for the next cycle continues until convergence is achieved.

3 ANALYSIS OF THREE-DIMENSIONAL TRIBOLOGICAL CHARACTERISTICS

Using the theoretical model presented above, simulation calculations were conducted for a certain type of high-power marine engine. Table 1 provides some structural parameters of the engine system, Table 2 lists the parameters required for establishing the mixed lubrication model. Figure 4 shows the inter-ring pressure curve, which was obtained using the method detailed in our previous study [34].

Table 1. Engine Structural Parameters

Parameter	Value
Density of piston rings	7850 (kg/m³)
Elastic modulus of piston rings	174 (GPa)
Poisson's ratio of piston ring	0.3 (-)
Bore of the cylinder liner	320 (mm)
Crank radius	210 (mm)
Rotate speed	750 (r/min)

Table 2. Parameters for the Mixed Lubrication Model

Parameter	Value
Composite surface roughness	2.1 (μm)
Maximum profile height	54 (μm)
Shear stress constant	2 (MPa)
Boundary friction coefficient	0.08 (-)

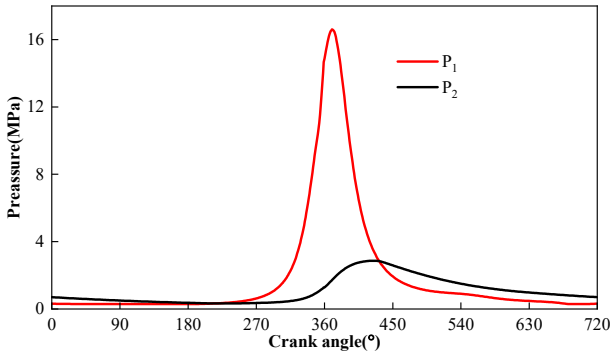

Figure 4. Inter-Ring Pressure Curve.

Figure 5(a) illustrates the evolution trend of piston ring mixed lubrication within 90°CA before and after the peak cylinder pressure: the closer to the top dead center (TDC), the larger the mixed lubrication region and the asperity contact force increases significantly. The asperity contact is most intense near the ring gap and the circumferential position at 0°.

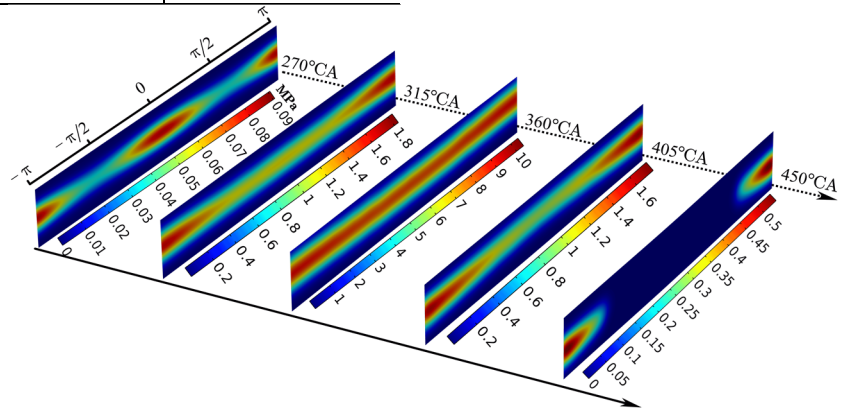

Figure 5. Evolution trend of mixed lubrication around TDC

As a pear-shaped elastic ring is used in this study, the elastic force at the piston ring's gap is relatively large, leading to the most severe wear near the gap. This result is consistent with the computational findings reported in existing literature. Furthermore, the wear on the piston ring is concentrated near the barrel peak of the ring profile, as the asperity contact pressure reaches its maximum in this region. It is evident that the wear of the three-dimensional piston ring exhibits significant circumferential non-uniformity, which cannot be fully accounted for by a two-dimensional model.

4 WEAR PREDICTION UNDER MULTI-SOURCE UNCERTAINTY

The wear of piston rings is often influenced by multiple sources of uncertainty. Based on the characteristics of the piston ring-cylinder liner friction pair, five key uncertain factors that significantly affect its failure were selected: wear coefficient, elastic force, composite roughness, rotational speed, and peak combustion pressure. Further, Latin Hypercube Sampling (LHS) was employed to generate 500 computational samples. The distributions of these uncertain factors are illustrated in Figure 6.

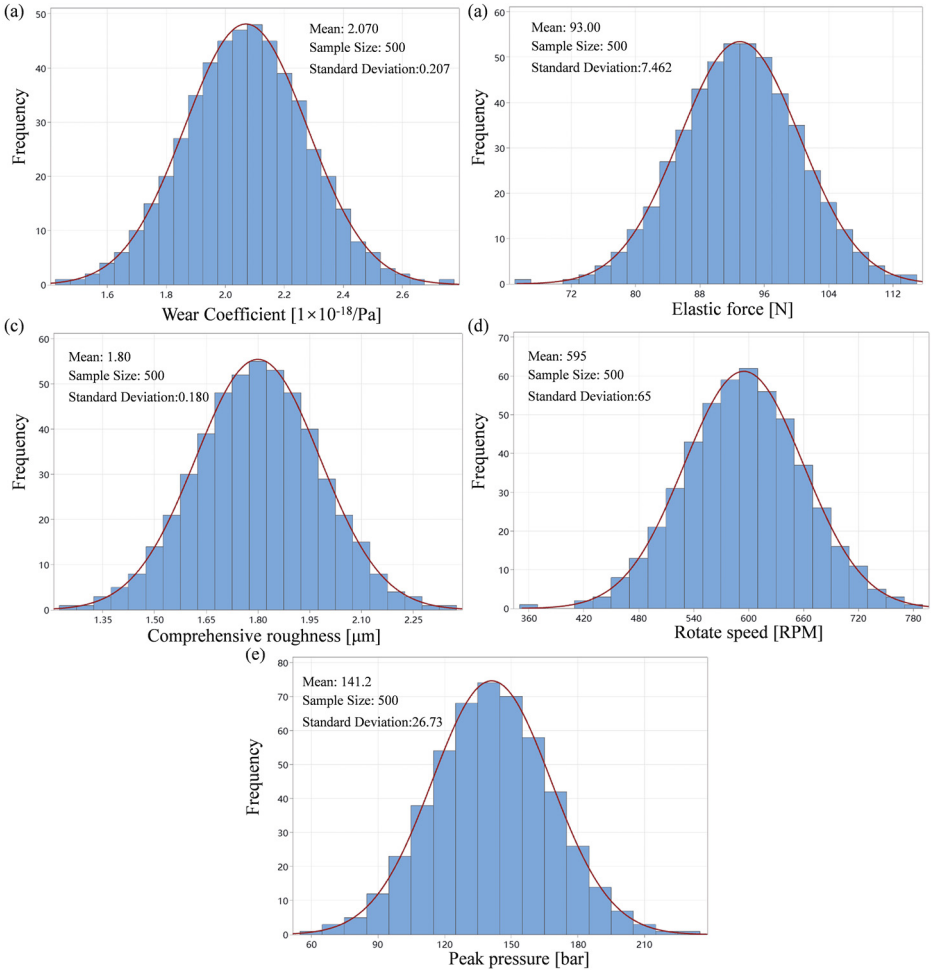

Figure 6. Distribution Forms of Uncertain Factors: (a) Wear coefficient; (b) Elastic force; (c) Composite roughness; (d) Rotational speed; (e) Peak pressure.

The above multidimensional random samples were input into the failure mechanism model for computation. Furthermore, based on the computational results of the random samples, the maximum wear per cycle was extracted as the object of reliability analysis. The statistical results of the maximum wear per cycle for each sample set are shown in Figure 7. From the figure, it can be observed that: (1) The variation range of the maximum wear per cycle is 0.9×10-6-2.7×10-6; (2) Probabilistic analysis indicates that the maximum wear per cycle follows a three-parameter Weibull distribution, as shown in Equation (15).

$$f(x)=\frac{\beta}{\alpha}\left(\frac{x-\mu}{\alpha}\right)^{\beta-1}\exp\left[-\left(\frac{x-\mu}{\alpha}\right)^{\beta}\right] \quad (15)$$

where β is the shape parameter, β =2.371. α is the scale parameter, α = 0.8083; μ is the location parameter, μ = 0.7819. x represents the single-cycle wear depth, with units of 1×10-6 μm/cycle.

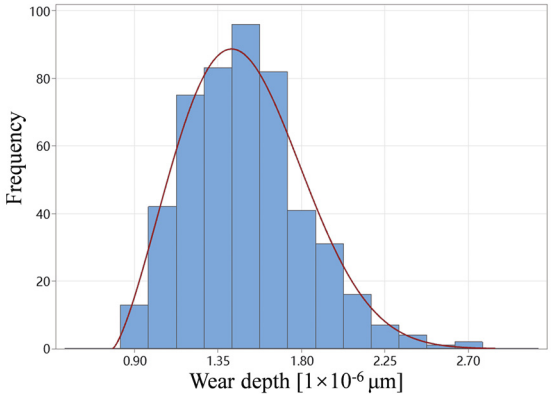

Figure 7. Distribution form of maximum wear depth

5 RELIABILITY ANALYSIS UNDER MULTI-SOURCE UNCERTAINTY

5.1 Wear prediction surrogate model

To establish the mapping relationship between the maximum wear depth and multiple sources of uncertainty, a wear prediction surrogate model was

developed. The Kriging model was selected to establish the relationship between multi-source uncertainties and the wear rate $h_{\max}(\mathbf{x})$ at the location of maximum wear. The selected Kriging model is shown in Equation (16) [35].

$$h_{\max}(\mathbf{x}) = h_t(\mathbf{x}) + \varepsilon \tag{16}$$

where $h_t(\mathbf{x})$ characterizes the variation trend of $h(\mathbf{x})$, and ε represents independent white noise $\varepsilon \sim N\left(0,\ \sigma_\varepsilon{}^2\right)$. Material parameters, elastic forces, and operating conditions are used as uncertain quantities $\mathbf{x} = \left(\mathbf{x}_1, \mathbf{x}_2, \mathbf{x}_3, \mathbf{x}_4, \mathbf{x}_5\right)$, with the corresponding maximum wear rate represented by $h_{\max}(\mathbf{x})$. For the latest input variable $\mathbf{x}^*$, the output h^* can be predicted. The mean and variance of the established Kriging model are shown in Equations (17) and (18) [35].

$$\begin{aligned} \mu_{h^*}\left(\mathbf{x}^*\right) &= \sigma^2 \mathbf{r}_*^\top \left(\sigma^2 \mathbf{R}_\mathbf{n} + \sigma_\varepsilon^2 I_n\right)^{-1} \mathrm{h}(\mathbf{x}) \\ &= \mathbf{r}_*^\top \left(\mathbf{R}_\mathbf{n} + \frac{\sigma_\varepsilon^2}{\sigma^2} I_n\right)^{-1} \mathrm{h}(\mathbf{x}) \end{aligned} \tag{17}$$

$$\begin{aligned} \sigma_{N^*}^2\left(\mathbf{x}^*\right) &= \sigma^2 - \sigma^2 \mathbf{r}_*^\top \left(\sigma^2 \mathbf{R}_\mathbf{n} + \sigma_\varepsilon^2 I_n\right)^{-1} \sigma^2 \mathbf{r}_* \\ &= \sigma^2 \left(1 - \mathbf{r}_*^\top \left(\mathbf{R}_\mathbf{n} + \frac{\sigma_\varepsilon^2}{\sigma^2} I_n\right)^{-1} \mathbf{r}_*\right) \end{aligned} \tag{18}$$

where $\mathbf{R}_\mathbf{n}$ and $\mathbf{r}_*$ are correlation matrixes, $\mathbf{R}_n = r\left(\mathbf{x}, \mathbf{x}\right) = \left(r\left(\mathbf{x}_i, \mathbf{x}_j\right)\right)$, $\mathbf{r}_* = r\left(\mathbf{x}, \mathbf{x}^*\right)$.

5.2 Reliability analysis of piston rings

Based on the calculation samples of input parameters, the surrogate model is used to calculate the damage (varying over time). For the damage samples at each time point, the parameters of the three-parameter Weibull distribution are fitted, and the relationship between the Weibull parameters and the input parameters is established. The damage samples at each time point are statistically analyzed, and the reliability at each time point is then calculated using the stress-strength interference theory.

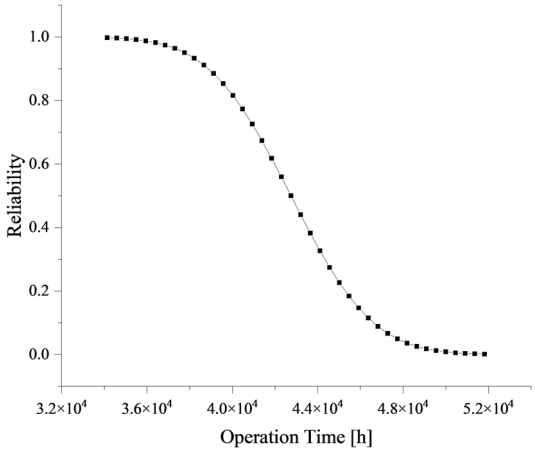

Figure 8. Reliability data

Table 3. Wear life of piston rings under different reliability

Reliability	0.99	0.95	0.9	0.85
Time/h	3.57×10^4	3.77×10^4	3.88×10^4	3.96×10^4

The reliability of the cylinder liner-piston ring under the calibrated operating conditions (750 r/min and a load factor of 1) is calculated, as shown in Figure 8. From the figure, it can be observed that the reliability of the cylinder liner-piston ring friction pair gradually decreases with the increase in operating time. Key reliability data at critical locations are presented in Table 3. When the reliability reaches 90%, the lifespan of the piston ring is approximately 3.88×10^4 hours.

6 CONCLUSIONS

(1) The wear of the three-dimensional piston ring exhibits significant circumferential non-uniformity, and the three-dimensional tribo-dynamic model provides a more comprehensive characterization and calculation of this phenomenon.

(2) Analysis reveals that when multi-source uncertainty factors follow a normal distribution, the single-cycle wear rate of the piston ring conforms to a three-parameter Weibull distribution.

(3) Further analysis shows that under the influence of multi-source uncertainties, the discrete range of the single-cycle wear depth is 0.9×10^{-6}-2.7×10^{-6} μm.

(4) Reliability analysis of the piston ring indicates that under the influence of multi-source uncertainties, the lifespan of the piston ring is approximately 3.96×10^4 hours at a reliability level of 85%.

7 REFERENCES AND BIBLIOGRAPHY

[1] Dowson D, Ruddy BL, Economou PN, Christopherson DG. The elastohydrodynamic lubrication of piston rings. Proc R Soc Lond Math Phys Sci 1997;386:409–30. https://doi.org/10.1098/rspa.1983.0043.

[2] Chu-Jung H, Cheng-I W. Elastohydrodynamic lubrication of piston rings. Wear 1991;150:203–15. https://doi.org/10.1016/0043-1648(91)90317-N.

[3] Gu C, Zhang D, Ding X, Wang S. A Model of Mixed Lubrication for the Repeated Sliding Problem Considering the Reloading Characteristic: Application to Ring/Liner Conjunction. J Tribol 2021;143:022201. https://doi.org/10.1115/1.4048271.

[4] Jiang YK, Zhang JP, Hong G, Wan LP, Liu X. 3D EHD lubrication and wear for piston ring-cylinder liner on diesel engines. Int J Automot Technol 2015;16:1–15. https://doi.org/10.1007/s12239-015-0001-x.

[5] Jiao B, Ma X, Wang Y, Lyu X, Li T, Liu Z. A fluid-structure coupled transient mixed lubrication model for piston ring lubrication property analysis with CMFF method. Int J Mech Sci 2023;252:108377. https://doi.org/10.1016/j.ijmecsci.2023.108377.

[6] Jiao B, Ma X, Wang Y, Liu Z, Li T, Lu X. Lubrication analysis of the piston ring for the two-stroke marine diesel engine based on modified radial tension. Int J Engine Res 2024;25:200–13. https://doi.org/10.1177/14680874231194390.

[7] Zhang H, Liu X, Gong J, Bai S, Sun K, Jia H. Thermohydrodynamic Lubrication Characteristics of Piston Rings in Diesel Engine Considering Transient Heat Transfer under the Parameterized Surface Texture of Cylinder Liners. Energies 2023;16:7924. https://doi.org/10.3390/en16247924.

[8] Chu NR, Jackson RL, Ghaednia H, Gangopadhyay A. A Mixed Lubrication Model of Piston Rings on Cylinder Liner Contacts Considering Temperature-Dependent Shear Thinning and Elastic–Plastic Contact. Lubricants 2023;11:208. https://doi.org/10.3390/lubricants11050208.

[9] Gu C, Meng X, Xie Y, Fan J. A thermal mixed lubrication model to study the textured ring/liner conjunction. Tribol Int 2016;101:178–93. https://doi.org/10.1016/j.triboint.2016.04.024.

[10] Harigaya Y, Suzuki M, Takiguchi M. Analysis of Oil Film Thickness on a Piston Ring of Diesel Engine: Effect of Oil Film Temperature. J Eng Gas Turbines Power 2003;125:596–603. https://doi.org/10.1115/1.1501078.

[11] Harigaya Y, Suzuki M, Toda F, Takiguchi M. Analysis of Oil Film Thickness and Heat Transfer on a Piston Ring of a Diesel Engine: Effect of Lubricant Viscosity. J Eng Gas Turbines Power 2004;128:685–93. https://doi.org/10.1115/1.1924403.

[12] Bahrom MZ, Manshoor B, Zaman I, Didane DH, Hang NW, Abdelaal MAS, et al. Numerical Analysis of Tribological Characteristics for Textured Piston Ring-Liners in Mixed Lubrication with A Non-Circular Cylinder Bore. J Complex Flow 2022;4:26–32.

[13] Gu C, Meng X, Zhang D. Analysis of the coated and textured ring/liner conjunction based on a thermal mixed lubrication model. Friction 2018;6:420–31. https://doi.org/10.1007/s40544-017-0176-4.

[14] Hu Y, Meng X, Xie Y, Fan J. Study on the frictional performance of slide and plateau honed cylinder liners during running-in. Ind Lubr Tribol 2017;69:282–99. https://doi.org/10.1108/ILT-02-2016-0026.

[15] Hu Y, Meng X, Xie Y. A new efficient flow continuity lubrication model for the piston ring-pack with consideration of oil storage of the cross-hatched texture. Tribol Int 2018;119:443–63. https://doi.org/10.1016/j.triboint.2017.11.027.

[16] Liu Z, Ning X, Meng X, Liao Q, Wang J. Starved lubrication analysis for the top ring and cylinder liner of a two-stroke marine diesel engine considering the thermal effect of friction. Int J Engine Res 2023;24:336–59. https://doi.org/10.1177/14680874211047923.

[17] Morris N, Rahmani R, Rahnejat H, King PD, Howell-Smith S. A Numerical Model to Study the Role of Surface Textures at Top Dead Center Reversal in the Piston Ring to Cylinder Liner Contact. J Tribol 2016;138. https://doi.org/10.1115/1.4031780.

[18] Delprete C, Razavykia A. Piston ring–liner lubrication and tribological performance evaluation: A review. Proc Inst Mech Eng Part J J Eng Tribol 2018;232:193–209. https://doi.org/10.1177/1350650117706269.

[19] Liu N, Wang C, Xia Q, Gao Y, Liu P. Simulation on the effect of cylinder liner and piston

ring surface roughness on friction performance. Mech Ind 2022;23:8. https://doi.org/10.1051/meca/2022007.

[20] Quan-bao Z, Tie-zhu Z, Rong-sheng W. A full lubrication model for rough surface piston rings. Tribol Int 1988;21:211–4. https://doi.org/10.1016/0301-679X(88)90019-9.

[21] Atulkar A, Pandey RK, Subbarao PMV. Performance analysis of two-dimensional section of partially textured piston ring with cavitation boundary conditions. Surf Topogr Metrol Prop 2021;9:025025. https://doi.org/10.1088/2051-672X/abfd05.

[22] Chong W, Teodorescu M, Vaughan N. Cavitation induced starvation for piston-ring/liner tribological conjunction. Tribol Int 2011;44:483–97. https://doi.org/10.1016/j.triboint.2010.12.008.

[23] De Boer G, Dowson D. An Arbitrary Lagrangian–Eulerian Formulation for Modelling Cavitation in the Elastohydrodynamic Lubrication of Line Contacts. Lubricants 2018;6:13. https://doi.org/10.3390/lubricants6010013.

[24] Dellis PS. Piston-ring performance: limitations from cavitation and friction. Int J Struct Integr 2019;10:304–24. https://doi.org/10.1108/IJSI-09-2018-0053.

[25] Gu C, Meng X, Xie Y, Zhang D. Mixed lubrication problems in the presence of textures: An efficient solution to the cavitation problem with consideration of roughness effects. Tribol Int 2016;103:516–28. https://doi.org/10.1016/j.triboint.2016.08.005.

[26] Patir N, Cheng H. An Average Flow Model for Determining Effects of Three-Dimensional Roughness on Partial Hydrodynamic Lubrication. J Lubr Technol 1978;100:12–7. https://doi.org/10.1115/1.3453103.

[27] Patir N, Cheng HS. Application of Average Flow Model to Lubrication Between Rough Sliding Surfaces. J Lubr Technol 1979;101:220–9. https://doi.org/10.1115/1.3453329.

[28] Lyu B, Meng X, Wang C, Cui Y, Wang C. Piston ring and cylinder liner scuffing analysis in dual-fuel low-speed engines considering liner deformation and tribofilm evolution. Int J Engine Res 2024:14680874241248878. https://doi.org/10.1177/14680874241248878.

[29] Lyu X, Hu J, Wang Y, Sheng J, Ma X, Li T, et al. Effect of temperature on tribofilm growth and the lubrication of the piston ring-cylinder liner system in two-stroke marine engines. Friction 2024. https://doi.org/10.1007/s40544-024-0872-9.

[30] Zhao Z, Shen Y, Liu Y, Xing C, Liu J, Fan J, et al. Low and high temperature effects on friction and wear performance of Cr-plated cylinder liner. Wear 2024;546–547:205329. https://doi.org/10.1016/j.wear.2024.205329.

[31] Greenwood JA, Tripp JH. The Contact of Two Nominally Flat Rough Surfaces. Proc Inst Mech Eng 1970;185:625–33. https://doi.org/10.1243/PIME_PROC_1970_185_069_02.

[32] Styles G, Rahmani R, Rahnejat H, Fitzsimons B. In-cycle and life-time friction transience in piston ring–liner conjunction under mixed regime of lubrication. Int J Engine Res 2014;15:862–76. https://doi.org/10.1177/1468087413519783.

[33] Leighton M, Nicholls T, De la Cruz M, Rahmani R, Rahnejat H. Combined lubricant–surface system perspective: Multi-scale numerical–experimental investigation. Proc Inst Mech Eng Part J J Eng Tribol 2017;231:910–24. https://doi.org/10.1177/1350650116683784.

[34] Gao L, Cui Y, Xu Z, Fu Y, Liu S, Li Y, et al. A fully coupled tribo-dynamic model for piston-ring-liner system. Tribol Int 2023;178. https://doi.org/10.1016/j.triboint.2022.107998.

[35] Zhan D, Xing H. A Fast Kriging-Assisted Evolutionary Algorithm Based on Incremental Learning. IEEE Trans Evol Comput 2021;25:941–55. https://doi.org/10.1109/TEVC.2021.3067015.

8 CONTACT

Lining Gao, Dr.

Shanghai Jiao Tong University, Shanghai, China

Mobil: 18817465350

E-mail: easoning@sjtu.edu.cn